ELSEVIER

Journal of Molecular Catalysis A: Chemical 155 (2000) 73–80

JOURNAL OF MOLECULAR CATALYSIS A: CHEMICAL

www.elsevier.com/locate/molcata

Direct decomposition of nitric oxide over stannate pyrochlore oxides: relationship between solid-state chemistry and catalytic activity

Yasutake Teraoka *, Ken-ichiro Torigoshi, Hidetoshi Yamaguchi, Takashi Ikeda, Shuichi Kagawa

Department of Applied Chemistry, Faculty of Engineering, Nagasaki University, Nagasaki 852-8521, Japan

Received 8 October 1998; accepted 1 February 1999

Abstract

Rare-earth stannate pyrochlores were synthesized and their NO decomposition activity was investigated in relation with the solid-state property. For pyrochlores free from transition metal substituents, $Ln_2Sn_2O_7$ (Ln = Y, La, Nd, Sm, Gd) and $La_{2-x}Ln'_xSn_2O_7$ (Ln′ = Nd, Sm), the strength of an Sn–O bond evaluated from its stretching IR band decreased almost linearly with increasing cubic cell parameter or the size of rare earth ions. The catalytic activity for the NO decomposition changed significantly with the sort of rare-earth ions, and oxides having the intermediate Sn–O bond strength showed the highest NO decomposition activity. For $La_2Sn_{1.9}M_{0.1}O_7$ (M = 3d transition metals, TM), the redox property of TMs was responsible for the NO decomposition activity, and the Co-substituted oxide showed the highest activity. Changes in activity for both the TM-free and TM-substituted systems were discussed on the basis of the redox-type reaction mechanism in which oxide ion vacancies are active sites. © 2000 Elsevier Science B.V. All rights reserved.

Keywords: Direct decomposition; Nitric oxide; Stannate pyrochlore oxides

1. Introduction

Mixed metal oxides represented by the general formula $A_2B_2O_7$ are oxide pyrochlores with good chemical and thermal stability: the exact formula is $A_2B_2O_6O'$ because there are two crystallographically nonequivalent sites for oxide ions. The larger A cation, usually 0.9–1.2 Å ionic radius, retains the eight-fold coordination (deformed cube), while the smaller B cation, 0.5–0.75 Å, is in six-fold coordination (deformed octahedron). Although both A^{3+}–B^{4+} and A^{2+}–B^{5+} combinations are possible, $A_2^{3+}B_2^{4+}O_7$ pyrochlores, in which A sites are usually occupied by rare earth ions, are common and large in number as compared to $A_2^{2+}B_2^{5+}O_7$. When criteria of the ionic radius and charge neutrality are satisfied, the partial substitution at A and B cationic sites as well as oxygen sites are possible. In addition, the crystal lattice tolerates vacancies at A and oxygen sites to a certain extent. By selecting A and B

* Corresponding author. Tel. and fax: +81-958-48-9652; e-mail: yasu@net.nagasaki-u.ac.jp

PII: S1381-1169(99)00320-9

cations and/or introducing lattice defects, oxide pyrochlores exhibit a wide variety of chemical and physical properties in ionic and electronic conduction, electrocatalysis, magnetic and dielectric behaviors, etc. [1]. These features in modifying the structure and property can be compared with those of perovskite-type oxides. However, in contrast with perovskites which have been investigated extensively and are important catalytic materials [2–4], the catalytic application of pyrochlores have been limited so far; e.g., CO–NO reaction [5], CO oxidation [5–7], N_2O decomposition [8] and oxidative coupling of methane [9–14].

This paper reports the synthesis, characterization and NO decomposition activity of rare-earth stannate pyrochlores with and without transition metal substitutes, and the catalytic activity is discussed in relation with solid-state chemistry.

2. Experimental

2.1. Synthesis of stannate pyrochlores

Acetates of rare-earth metals, nitrates of 3d transition metals, and hydrous SnO_2 were used as starting materials. Hydrous SnO_2 was obtained by adding aqueous ammonia to an aqueous solution of $SnCl_4$, followed by filtration, washing with deionized water, and drying at 110°C. Hydrous SnO_2 was added into an aqueous solution containing a rare earth ion and optionally a transition metal, and the suspended solution was evaporated to dryness under vigorous stirring. The obtained solid was ground, heat-treated at 400°C for 3 h, and calcined at 900 or 950°C for 10 h in air.

2.2. Characterization

Crystal structure of products was analyzed by X-ray diffraction (XRD) technique with CuKα radiation (Rigaku RINT2200). Infrared (IR) spectra were recorded on Perkin-Elmer 1650 FTIR spectrometer in the transmission mode (KBr method). Temperature-programmed desorption (TPD) of oxygen was carried out by heating a sample in a helium stream and the desorbed oxygen was monitored by a thermal conductivity detector (TCD). Temperature-programmed reduction (TPR) was performed by heating a sample in a stream of $2\%H_2/N_2$ and the consumed H_2 was monitored by TCD. The programmed heating rate was 10°C min^{-1} for both cases. Before subjecting TPD and TPR experiments, samples were pretreated with O_2 by cooling them from 800°C to RT in an O_2 atmosphere (100 Torr).

2.3. Catalytic activity measurement

The catalytic activity for NO decomposition was measured with a fixed-bed flow reactor by feeding NO(1%)–He(balance) gas at a rate of 15 cm^3 min^{-1} over 1 g of a catalyst ($W/F = 4.0$ g s cm^{-3}). The NO decomposition activity was evaluated in terms of the conversion of NO into N_2, $X(N_2)/\% = \{2[N_2]_{out}/[NO]_{in}\} \times 100$, and the rate of N_2 formation per surface area, $R(N_2)$/nmol m^{-2} s^{-1}.

3. Results and discussion

3.1. Synthesis and structural characterization of stannate pyrochlores

Single-phase pyrochlore oxides containing rare-earth (Ln) ions and Sn^{4+} are listed in Table 1. All the oxides crystallized in a cubic pyrochlore structure. In order to introduce oxide ion vacancies, synthesis of Sr-substituted oxides, $Ln_{2-x}Sr_xSn_2O_{7-(x/2)}$ (Ln = La, Sm, Gd, $x = 0.2$, 0.6), was tried, but the impurity phase of $SrSnO_3$ was always formed and could not be disappeared under the present preparation condition. On the contrary, $La_2Sn_{1.9}M_{0.1}O_7$ (M = 3d transition metals, TM) could be obtained as single-phase cubic pyrochlore oxides. It is expected that TM-substituted stannate pyrochlores have a nonstoichiometric composition if the oxidation number of a TM ion is lower than that of Sn (4 +). In this sense, the oxides should be

Table 1
List of rare-earth stannate pyrochlores with their cubic cell parameter (a) and specific surface area (S_a)

Pyrochlores	a (Å)	S_a ($m^2\ g^{-1}$)
$Ln_2Sn_2O_7$		
(1) $La_2Sn_2O_7$	10.698	15.0
(2) $Nd_2Sn_2O_7$	10.570	13.6
(3) $Sm_2Sn_2O_7$	10.504	7.0
(4) $Gd_2Sn_2O_7$	10.437	5.0
(5) $Y_2Sn_2O_7$	10.355	21.0
$La_{2-x}Sm_xSn_2O_7$		
(6) $x = 0.25$	10.669	7.4
(7) 0.5	10.643	7.6
(8) 0.75	10.648	15.1
(9) 1.0	10.604	3.2
(10) 1.5	10.534	27.2
$La_{2-x}Nd_xSn_2O_7$		
(11) $x = 0.25$	10.644	10.5
(12) 1.0	10.599	14.5
(13) 1.5	10.576	7.5
$La_2Sn_{1.9}M_{0.1}O_7$		
(14) M = Cr	10.696	13.2
(15) Mn	10.682	8.8
(16) Fe	10.673	6.7
(17) Co	10.692	1.3
(18) Ni	10.661	7.7
(19) Cu	10.698	1.3

expressed by $La_2Sn_{1.9}M_{0.1}O_{7-\delta}$ (δ = oxygen deficiency), but a nominal formula $La_2Sn_{1.9}M_{0.1}O_7$ is used instead for simplicity.

The relation between the cubic cell parameter, a, and an ionic radius of Ln ion in 8-fold coordination [15], r(Ln), is depicted in Fig. 1 for $Ln_2^{3+}Sn_2^{4+}O_7$ (1–13; Ln = La–Y, La/Nd and La/Sm) which should have stoichiometric composition. In cases of $La_{2-x}Ln'_xSn_2O_7$ (Ln′ = Nd, Sm), an average ionic radius of r(La) and r(Ln′) were used; $\{(2-x)r(La) + xr(Ln')\}/2$. The a value of $Ln_2Sn_2O_7$ (Ln = La, Nd, Sm, Gd, Y) increased linearly with an increase in the ionic radius of Ln ion, as expected (Fig. 1). In addition, cell parameters of mixed rare earth systems (La/Nd, La/Sm) were practically on the correlation line, indicating that La and Ln′ ions randomly occupy A sites to form homogeneous solid solution phases. For TM-substituted series, on the other hand, no

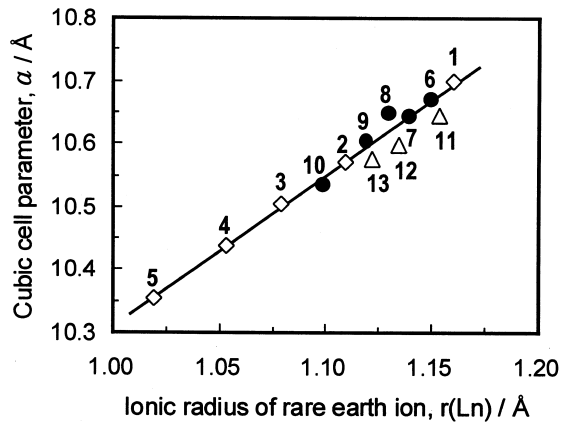

Fig. 1. Cubic cell parameter of stannate pyrochlores as a function of ionic radius of rare-earth ion. See Table 1 for the listing of catalysts.

systematic change of the a value with the ionic radius of TM ion was observed probably due to the effect of oxide ion vacancies.

It has been reported that pyrochlore oxides exhibit seven IR bands in the range of 750–50 cm^{-1} originating from vibration and bending of metal–oxygen bonds [1]. Fig. 2 shows IR spec-

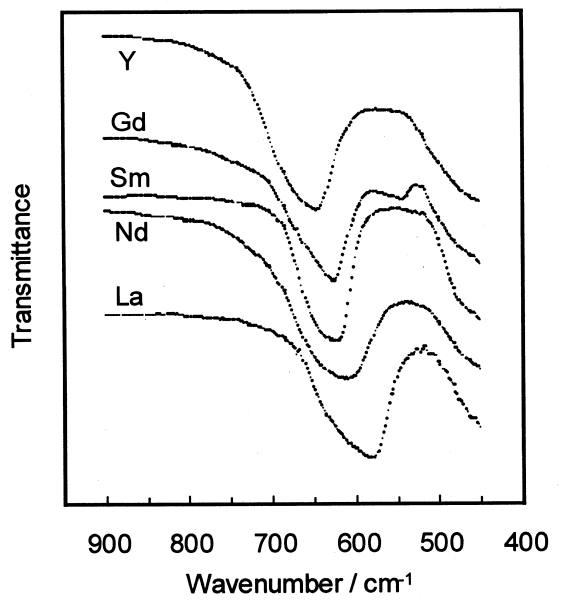

Fig. 2. Infrared spectra of the Sn–O stretching vibration of $Ln_2Sn_2O_7$ (Ln = La, Nd, Sm, Gd, Y).

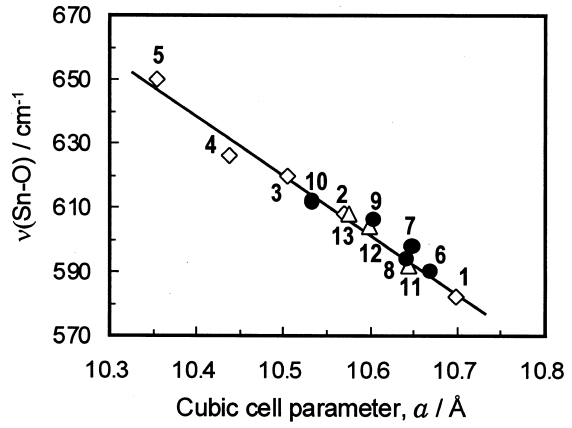

Fig. 3. Relation between the frequency (in cm^{-1}) of the Sn–O vibration IR band, ν(Sn–O), and the cubic cell parameter of stannate pyrochlores. See Table 1 for the listing of catalysts.

tra of single rare earth $Ln_2Sn_2O_7$ in the range of 900–450 cm^{-1}; it was impossible with our instrument to record IR spectra below 450 cm^{-1}. In this region, only one broad band ascribable to Sn–O stretching vibration [1,16] was observed for each sample, and the frequency of the band maximum, ν(Sn–O), progressively increased on passing from La to Y. In Fig. 3, the ν(Sn–O) value is plotted against the cubic cell parameter for both single and mixed rare earth systems. The ν(Sn–O) value decreased almost linearly with increasing the a value, or r(Ln) (cf. Fig. 1), indicating that the Sn–O bond strength weakens with an increase in a or r(Ln). This is basically in accordance with the calculated Sn–O bond energy for $Ln_2Sn_2O_7$ (Ln = Gd, Ho, Sm, Y, Eu, Dy, Nd, La) reported by Petit et al. [10,11]. The calculated bond energy decreased with an increase in r(Ln) excepting for Y and Eu. The change in the Sn–O bond strength might be ascribable to that of the bond distance, because the Sn–O bond distance of rare earth stannate pyrochlores is reported to increase monotonically with increasing a or r(Ln) [17].

3.2. Oxygen desorption and reduction behaviors

It is expected that the difference in the Sn–O bond strength affects behaviors of oxygen desorption and reduction. This was examined by temperature programmed desorption of oxygen (TPD) and temperature programmed reduction (TPR) by H_2 for selected samples with different Sn–O bond strength; $Ln_2Sn_2O_7$ (Ln = La, Nd, Sm), $La_{1.75}Nd_{0.25}Sn_2O_7$ and $La_{1.25}Sm_{0.75}Sn_2O_7$. TPD chromatogram of oxygen from $La_2Sn_2O_7$ is depicted in Fig. 4. Oxygen desorption started around 300°C and after exhibiting a plateau-like peak the desorption rate increased again above 600°C. This oxygen desorption behavior was basically common to all the samples examined. The amount of oxygen desorbed from $La_2Sn_2O_7$ below 800°C is approximately 0.2% of total bulk oxygen or 19% of the surface oxygen; one surface layer is assumed to be 16.0 μmol-O m^{-2} which is an average value of (100) and (110) planes. Accordingly, the desorbed oxygen is reasonably ascribable to adsorbed oxygen and lattice oxygen in the vicinity of the surface. TPR profiles of all the samples were very similar in shape. The reduction started around 200°C and a plateau-like peak was observed up to ca. 500°C: oxygen removed from $La_2Sn_2O_7$ under the peak amounted to approximately 3% and 300% of bulk and surface oxygen, respectively. Above 500°C, the reduction rate became faster and the amount of removed oxygen increased

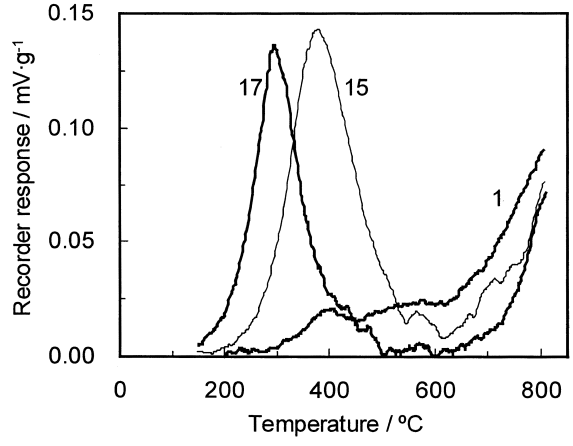

Fig. 4. Temperature-programmed desorption of oxygen from $La_2Sn_2O_7$ (1), $La_2Sn_{1.9}Mn_{0.1}O_7$ (15) and $La_2Sn_{1.9}Co_{0.1}O_7$ (17).

almost linearly up to, for example, 20% of bulk oxygen of $La_2Sn_2O_7$. As shown in Fig. 5, both the amount of oxygen desorbed (TPD) and that of removed in the plateau-like peak (TPR) tended to decrease with an increase in ν(Sn–O). This is reasonable because the removal of oxide ions should become difficult with increasing the Sn–O bond strength.

When transition metal ions were replaced for Sn ions, the oxygen desorption and reduction behaviors were strongly modified. As shown in Fig. 4, $La_2Sr_{1.9}M_{0.1}O_7$ showed desorption peaks centered at 290°C (M=Co) and 380°C (Mn) in addition to the O_2 desorption above 600°C which is intrinsic to the La–Sn pyrochlore. The enhancement of the reducibility by introducing TMs was also confirmed by TPR. These results clearly show that TM-substituted oxides acquire the larger redox capacity due to the intrinsic redox property of substituted TM ions and/or the formation of oxide ion vacancies.

3.3. NO decomposition activity

Fig. 6 shows the temperature dependence of NO decomposition activity of selected stannate pyrochlores. The activity appeared above 500°C and increased monotonically with an increase in temperature, which is similar to that of perovskite-type oxides [18,19]. Stannate pyrochlores free from transition metals showed the different NO decomposition activity depending on the sort of Ln ions. Since neither SnO_2 nor La_2O_3 showed the activity under the present experimental conditions, the formation of pyrochlore oxides is indispensable for the appearance of the NO decomposition activity. The effect of the TM substitution was demonstrated by comparing the activity between $La_2Sn_2O_7$ (1) and $La_2Sn_{1.9}Co_{0.1}O_7$ (17). When the activ-

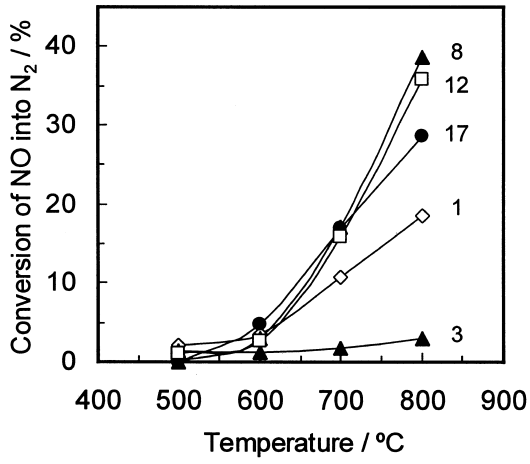

Fig. 6. Temperature dependence of NO decomposition activity of stannate pyrochlores. (1) $La_2Sn_2O_7$, (3) $Sm_2Sn_2O_7$, (8) $La_{1.25}Sm_{0.75}Sn_2O_7$, (12) $LaNdSn_2O_7$, (17) $La_2Sn_{1.9}Co_{0.1}O_7$.

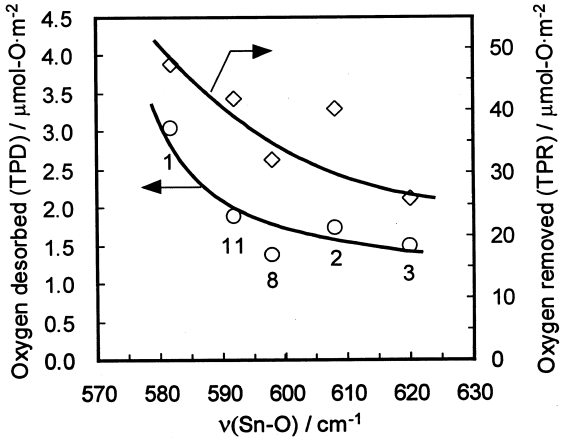

Fig. 5. The amounts of oxygen desorbed in TPD and removed in TPR as a function of the frequency of the Sn–O vibration IR band, ν(Sn–O), of $Ln_2Sn_2O_7$. Ln_2; (1) La_2, (2) Nd_2, (3) Sm_2, (8) $La_{1.25}Sm_{0.75}$, (11) $La_{1.75}Nd_{0.25}$.

ity is normalized to surface area ($X(N_2)$/specific surface area), the most active pyrochlore among the TM-free oxides is $La_{1.25}Sm_{0.75}Sn_2O_7$ (2.6% m^{-2} at 800°C) and that among the TM-substituted oxides is $La_2Sn_{1.9}Co_{0.1}O_7$ (22.0% m^{-2}). It is noted that $La_2Sn_{1.9}Co_{0.1}O_7$ is more active than $La_{0.8}Sr_{0.2}CoO_3$ which is the most active perovskite catalyst and have the specific activity of 9–12% m^{-2} at 800°C [18,19].

The rates of N_2 formation at 800°C over TM-free stannates are plotted against ν(Sn–O) in Fig. 7. The specific activity displayed the volcano-shape dependence on ν(Sn–O) irrespective of the A-site composition (single or mixed), and oxides having the intermediate ν(Sn–O) or the intermediate Sn–O bond strength showed highest NO decomposition activity.

The effect of substitution of TM ions for Sn is depicted in Fig. 8. The conversion of NO became highest at Mn- and Co-substituted oxides, and specific activity per surface area was greatly enhanced by the substitution of Co. For redox-type reactions, maxima of activity were generally observed for Mn and Co over simple oxides of TMs [20] and TM-containing perovskites [21]. This activity pattern is also found in Fig. 8, and therefore the redox property of TMs is of primary importance in the TM-substituted stannate pyrochlores.

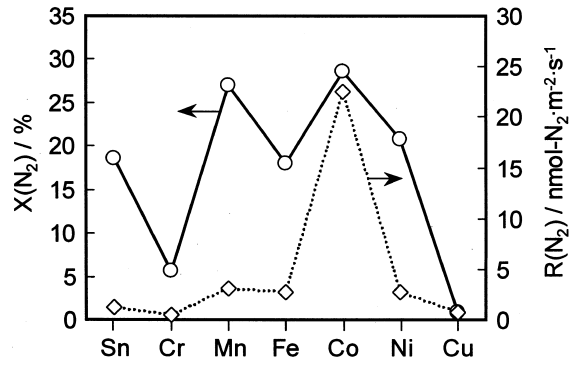

Fig. 8. NO decomposition activity at 800°C of $La_2Sn_{1.9}M_{0.1}O_7$ (M = Sn, Cr, Mn, Fe, Co, Ni, Cu). $X(N_2)$; conversion of NO into N_2, $R(N_2)$; rate of N_2 formation.

3.4. Reaction scheme of NO decomposition

It has been reported that, over mixed and simple metal oxides, the active site for NO decomposition is oxide ion vacancies (V_O) and that the step of N_2 formation is fast [22–24]. Fig. 9 is a plausible reaction scheme of NO decomposition over rare earth stannate, which consists of the oxygen-uptake step into V_O (I) and oxygen-desorption step to regenerate V_O sites (II). Under the mechanism, the activity is determined by the metal–oxygen bond strength and the redox property of metal ions. In case of TM-free stannates (M=Sn in Fig. 9), the step I (Sn–O bond formation) becomes easier while

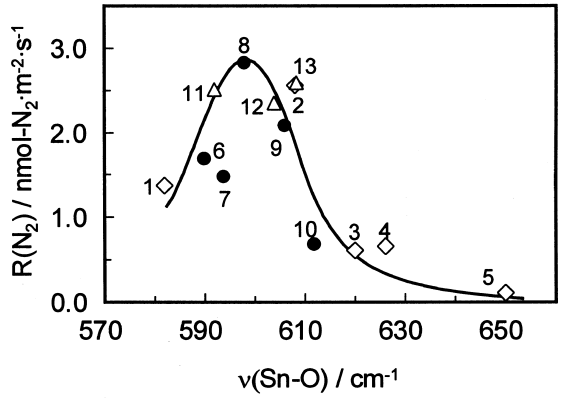

Fig. 7. Rate of N_2 formation at 800°C, $R(N_2)$, as a function of the frequency of the Sn–O vibration IR band, ν(Sn–O), of $Ln_2Sn_2O_7$. See Table 1 for the listing of catalysts.

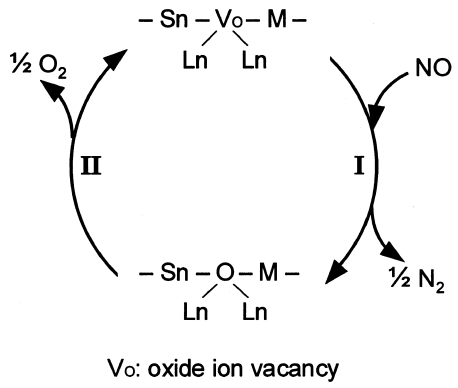

Fig. 9. Plausible reaction scheme of NO decomposition over stannates pyrochlores. M represents Sn and transition metals, respectively, for pyrochlores without and with transition metal substitutes.

the step II (Sn–O bond breaking) does more difficult with increasing the Sn–O bond strength. Accordingly, oxides with the intermediate Sn–O bond strength, on which both I and II steps proceed at reasonable rates, show highest NO decomposition activity (Fig. 7). In this sense, the formation of mixed rare earth pyrochlores is very significant, because the Sn–O bond strength can be adjusted to an appropriate value by the combination and composition of rare-earth ions ($La_{1.25}Sm_{0.75}$ in the present study).

As for TM-substituted oxides (M=TM in Fig. 9), on the other hand, the uptake and desorption of oxygen at V_O sites is regulated mainly by the substituted TM ions because the redox change of TM ions is easier than that of Sn ions (cf. TPD results in Fig. 4). In this case, the redox property of TM ions, rather than Sn–O bond strength, is responsible for the NO decomposition activity as shown in Fig. 8 and discussed above.

4. Conclusions

For stannate pyrochlores free from transition metal substituents, the Sn–O bond strength evaluated from the stretching IR band decreased almost linearly with increasing cubic cell parameter or the size of rare earth ions. The amount of oxygen thermally desorbed and removed by H_2 decreased with an increase in the Sn–O bond strength. The catalytic activity for the NO decomposition showed the volcano-shape dependence on the Sn–O bond strength, attaining the highest activity with $La_{1.25}Sm_{0.75}Sn_2O_7$ having the intermediate Sn–O bond strength. This result could be explained on the basis of redox-type reaction mechanism in which oxide ion vacancies serve as active sites. The activity of $La_2Sn_2O_7$ changed significantly by the partial substitution of 3d transition metals (TMs) for Sn ($La_2Sn_{1.9}M_{0.1}O_7$), and was enhanced by the substitution of Mn and especially Co. For TM-substituted stannate pyrochlores, the redox property of TMs was responsible for the NO decomposition activity rather than the Sn–O bond strength.

Acknowledgements

This study was partly supported by a Grant-in-Aid from the Ministry of Education, Science, Sports and Culture of Japan.

References

[1] M.A. Subramania, G. Aravamudam, G.V. Subba Rao, Prog. Solid State Chem. 15 (1983) 55.
[2] L.G. Tejuca, J.L.G. Fierro, J.M.D. Tascón, Adv. Catal. 36 (1989) 237.
[3] N. Yamazoe, Y. Teraoka, Catal. Today 8 (1990) 175.
[4] L.G. Tejuca, J.L.G. Fierro (Eds.), Properties and Applications of Perovskite-type Oxides, Mercel Dekker, New York, 1993.
[5] J.B. Goodenough, R.N. Castellano, J. Solid State Chem. 44 (1982) 108.
[6] J.H.H. ter Maart, M.P. van Dijk, G. Roelofs, H. Bosch, G.M.H. van de Velde, P.J. Gellings, A.J. Burggraaf, Mater. Res. Bull. 19 (1984) 1271.
[7] S.J. Korf, J.A. Koopmans, B.C. Lippens Jr, A.J. Burggraaf, P.J. Gellings, J. Chem. Soc., Faraday Trans. I (83) (1987) 1485.
[8] J. Christopher, C.S. Swammy, J. Mater. Sci. 26 (1991) 4966.
[9] A.T. Ashcroft, A.K. Cheethman, M.L.H. Green, C.P. Grey,

P.D.F. Vernon, J. Chem. Soc., Chem. Commun., 1989, p. 1667.
[10] C. Petit, J.L. Rehspringer, A. Kaddouri, S. Libs, P. Poix, A. Kiennemann, Catal. Today 13 (1992) 409.
[11] C. Petit, A. Kaddouri, S. Libs, A. Kiennemann, J.L. Rehspringer, P. Poix, J. Catal. 140 (1993) 328.
[12] A.C. Roger, C. Petit, L. Hilaire, J.-L. Rehspringer, A. Kiennemann, Catal. Today 21 (1994) 341.
[13] C.A. Mims, A.J. Jacobson, R.B. Bell, J.T. Lewandowski Jr., J. Catal. 153 (1995) 197.
[14] A.C. Roger, C. Petit, A. Kiennemann, J. Catal. 167 (1997) 447.
[15] R.D. Shannon, Acta Cryst. A 32 (1976) 751.
[16] J.F. McCaffery, N.T. McDevitt, C.M. Philippi, J. Opt. Soc. Am. 61 (1971) 209.
[17] B.J. Kennedy, B.A. Hunter, C.J. Howard, J. Solid State Chem. 130 (1997) 58.
[18] Y. Teraoka, H. Fukuda, S. Kagawa, Chem. Lett. (1990) p. 1.
[19] Y. Teraoka, T. Harada, H. Furukawa, S. Kagawa, Stud. Surf. Sci. Catal. 75 (1993) 2649.
[20] L.A. Sazonov, Z.V. Moskvina, E.V. Artamonov, Kinet. Katal. 15 (1974) 120.
[21] G. Kremenic, J.M.L. Nieto, J.M.D. Tascón, L.G. Tejuca, J. Chem. Soc., Fadaray Trans. I (81) (1985) 939.
[22] E.R.S. Winter, J. Catal. 22 (1971) 158.
[23] S. Shin, H. Arakawa, Y. Hatakeyama, K. Ogawa, K. Shimomura, Mater. Res. Bull. 14 (1979) 633.
[24] Y. Teraoka, T. Harada, S. Kagawa, J. Chem. Soc., Faraday Trans. 94 (1998) 1887.